Structure, energetics and vibrational spectra of protonated chlortetracycline in the gas phase: An experimental and computational investigation

ARTICLE *in* INTERNATIONAL JOURNAL OF MASS SPECTROMETRY · APRIL 2012

Impact Factor: 1.97 · DOI: 10.1016/j.ijms.2012.02.025

5 AUTHORS, INCLUDING:

Blake E Ziegler
University of Waterloo
9 PUBLICATIONS **33** CITATIONS
SEE PROFILE

Sabrina Martens
University of Waterloo
6 PUBLICATIONS **18** CITATIONS
SEE PROFILE

Jonathan K Martens
Radboud University Nijmegen
15 PUBLICATIONS **75** CITATIONS
SEE PROFILE

Terrance Mcmahon
University of Waterloo
206 PUBLICATIONS **5,438** CITATIONS
SEE PROFILE

International Journal of Mass Spectrometry xxx (2012) xxx–xxx

Contents lists available at SciVerse ScienceDirect

International Journal of Mass Spectrometry

journal homepage: www.elsevier.com/locate/ijms

Structure, energetics and vibrational spectra of protonated chlortetracycline in the gas phase: An experimental and computational investigation

Blake E. Ziegler, Rick A. Marta, Sabrina M. Martens, Jonathan K. Martens, Terry B. McMahon*

Department of Chemistry, University of Waterloo, Waterloo, Ontario, Canada N2L 3G1

ARTICLE INFO

Article history:
Received 31 October 2011
Received in revised form 26 February 2012
Accepted 27 February 2012
Available online xxx

Keywords:
Tetracylcine
IRMPD
Gaseous ion structure
Gaseous ion thermochemistry
Electronic structure calculations

ABSTRACT

Infrared Multiple Photon Dissociation (IRMPD) Spectroscopy has been used to generate gas phase vibrational spectra for six protonated tetracycline derivatives: chlortetracycline, meclocycline, minocycline, doxycycline, tetracycline, and metacycline. The IRMPD spectrum for protonated chlortetracycline is compared here to theoretical gas phase vibrational spectra obtained from geometry optimization and frequency electronic structure calculations using the B3LYP hybrid density functional method with the 6-311+G(d,p) basis set. The most energetically favorable protonation sites, tautomer structures, and hydrogen bond orientations were determined. Protonation at the dimethyl amine functional group and an extensive hydrogen bonding network lead to the most energetically favourable structures. Calculated spectra directly resembled the IRMPD spectrum, supporting the conclusion that the probable gas phase structure of protonated chlortetracycline has been determined.

1. Introduction

The tetracyclines are a class of antibiotics first discovered in 1948 [1]. Chlortetracycline was among the initial compounds investigated from this class which was isolated from *Streptomyces aureofaciens* [2]. Soon after, other tetracycline derivatives were characterized from either natural sources or synthetic method products. One such natural derivative was tetracycline, discovered in 1953 as a naturally occurring compound isolated from *S. aureofaciens*, *Streptomyces rimosus*, and *Streptomyces viridofaciens* [3]. Afterward, metacycline, doxycycline, and minocycline were discovered as a result of functional group substitution of known naturally occurring tetracyclines *via* synthetic organic chemistry techniques [4–6]. Although these initial compounds adequately fulfilled their purpose as potent antimicrobials, new synthetic or natural variations were sought in order to increase solubility in water, thus yielding supposedly increased therapeutic effectiveness due to enhanced intestinal absorption [7]. Surprisingly, despite the abundance of tetracycline derivatives (~1000), only a select few are therapeutically useful as antimicrobials [8].

Tetracyclines are commonly referred to as broad spectrum agents because they have antibiotic activity against chlamydiae, rickettsiae, mycoplamas, protozoans, and, importantly, both gram positive and negative bacteria [9]. Since tetracyclines are relatively safe due to a lack of significant side-effects, they have been widely used in humans and animals. These molecules have even been added to feed stocks to promote the growth of commercial farm animals such as cows and pigs. Unfortunately, the overuse of tetracyclines as antibacterials has led to the development of microbial resistance, thus reducing their effectiveness and hindering an important tool to sustain human life through the combat of detrimental organisms [10].

The structure of tetracycline molecules has been well established in order to decipher the structural features resulting in antibiotic action. The chemical structure of tetracycline derivatives is commonly represented in the form shown in Fig. 1. The R1, R2, and R3 functional groups differ in each derivative to give physical and, to some extent, biological properties. All tetracycline molecules are comprised of 4 linear fused hexacarbocyclic rings, however there are many variants due to the functional groups bonded to the 4 fused rings which constitute the various derivatives and are well described in the literature [7–10]. As pharmacological agents, tetracyclines typically exist as the hydrochloride salts in which the tetracycline structure is protonated to form the cation of the salt. X-ray crystal structure studies have revealed that in all cases protonation occurs at the dimethyl amine moiety, which is common to all tetracycline derivatives [11,12].

The antibacterial activity of the tetracyclines results from their ability to inhibit the formation of the bacterial ribosome and aminoacyl-tRNA complex needed to translate bacterial proteins essential for the sustainment of bacterial cell life [7–10].

As part of an ongoing effort in our laboratory to relate energetics and structure of biologically relevant molecules to their chemical and biological activity, we have undertaken a study of a series of

* Corresponding author. Tel.: +1 519 888 4591; fax: +1 519 746 0435.
E-mail address: mcmahon@uwaterloo.ca (T.B. McMahon).

1387-3806/$ – see front matter © 2012 Elsevier B.V. All rights reserved.
doi:10.1016/j.ijms.2012.02.025

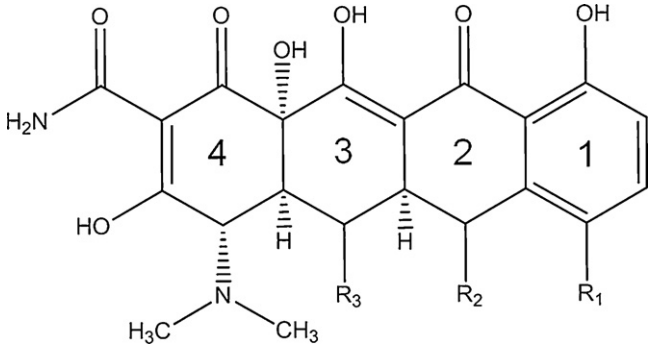

Fig. 1. Common representation of typical molecules of the tetracycline class. The R1, R2, and R3 groups differ among the tetracycline derivatives.

protonated tetracyclines using Infrared Multiple Photon Dissociation (IRMPD) and quantum chemical calculations. In particular, protonated chlortetracycline, meclocycline, minocycline, metacycline, tetracycline, and doxycycline have been investigated as key examples of this interesting class of molecules. The present work describes a detailed structural and energetic analysis of chlorotetracycline as a representative example.

2. Experimental and computational

Electronic structure calculations were performed using the *Gaussian 09* program package [13]. Structural optimizations and frequency calculations were obtained at the B3LYP/6-311 + G(d,p) level of theory [14]. This level of theory has been shown to be a relatively low computational cost yet high accuracy method of calculating vibrational frequencies [6,15–18] and optimized structures for gaseous ionic complexes which exhibit hydrogen bonding [16,17,19]. Harmonic frequencies have been scaled by a factor of 0.9688 to account for systematic errors arising from using a harmonic oscillator approximation and long range interactions [20]. Computed vibrational spectra were generated using a Lorentzian line shape with a full width at half maximum of 15 cm^{-1}.

Further calculations were completed using the Self-consistent Reaction Field (SCRF) method with the Polarizable Continuum Model in order to determine energetics of the various species in water solvent. These were also performed using the B3LYP method at the 6-311 + g(d,p) level of theory.

The use of IRMPD and electronic structure calculations for the characterization of structures of biologically relevant gaseous ions is well established [21–33]. In this work IRMPD spectroscopy was used in order to obtain the gas phase infrared spectra of the six protonated tetracycline derivatives of this study. IRMPD spectroscopy is a technique that allows for the generation of infrared absorption consequence data from mass-selected gas phase molecular ions. Therefore, a spectrum can be generated by calculating the efficiency of fragmentation induced by the absorption of specific photon energies, where the fragmentation efficiency is shown in Eq. (1), in which p_{frag} represents the fragmentation efficiency, I_{parent} represents the intensity of the parent ion, and $\Sigma I_{fragment}$ represents the sum of the intensities of the fragments of the parent ion generated as a result of IRMPD.

$$p_{frag} = -\log\left[\frac{I_{parent}}{I_{parent} + \Sigma I_{fragment}}\right] \quad (1)$$

IRMPD experiments were carried out at the Centre de Laser Infrarouge d'Orsay (CLIO) at the University of Paris XI. The free electron laser [34] produces a pulse train consisting of micropulses of approximately 1 ps in width with a spacing of 16 ns. Macropulses consist of roughly 6000 micropulses which are comprised of bunches 10 μs in width with a spacing of approximately 40 ms. These macropulses are then admitted to the ion trap. The 16 ns spacing of the micropulses is such that sufficient time is available for intramolecular vibrational redistribution (IVR) to readily occur.

Solutions containing protonated chlorotetracycline were prepared with concentrations of ~10^{-5} to 10^{-6} M in 50:50 acetonitrile and water with 0.1% formic acid. The ionic species of interest were generated using electrospray ionization and the ions were subsequently transferred to a Bruker Esquire ion trap mass spectrometer where the desired ionic species is mass isolated, trapped and irradiated by the tunable IR beam of the free electron laser. Sequential multiple photon absorption followed by fragmentation thus generates a consequence spectrum, which, as a function of wavelength, gives the IRMPD vibrational spectrum.

3. Results and discussion

As a starting point for the structural investigations it is of interest to examine the structures of neutral (unprotonated) and protonated chlorotetracycline deemed to be present in previous experimental work in solid state and solution. Crystal structure studies of the neutral form [35] (Fig. 1) suggest that the exocyclic oxygens of rings 1 and 3 are enolic while that of ring 2 is a carbonyl. Ring 4 consists of an exocyclic carbonyl oxygen adjacent to the ring junction with ring 3 and on the same side of the molecule as the other exocyclic oxygens of rings 1, 2 and 3. Further, ring 4 has an amide moiety on the carbon adjacent to the carbonyl, and an enol functionality, as well as the dimethylamino substituent. Solid state crystal structural analysis [36] as well as solution phase NMR experiments [37–39] show that the hydrochloride salt of chlorotetracycline exhibits much the same structure, although the NMR studies do suggest the possibilities of two intramolecular hydrogen bonds. The first of these involves a rotation of the amide group to give intramolecular hydrogen bonding between an amide amino hydrogen and the carbonyl oxygen of ring 4 while the second arises from the enol hydrogen and the carbonyl oxygen of the amide group. In addition, enolization of the amide functionality is also suggested as a possibility for tetracyclines in general.

Computational investigations of the structure and energetics of numerous isomers and tautomers of protonated chlorotetracycline have been carried out. The relative energetics of the seven most energetically favourable structural variants of chlorotetracycline are summarized in Table 1. For the discussion of structures and energetics, only those structures found to lie within100 kJ mol^{-1} in free energy at 298 K of the most stable structure have been considered. Even though many other possible protonation sites were explored, none were found to approach the stability of those

Table 1
Relative energetics of chlortetracycline structures protonated at various positions calculated at the B3LYP/6-311 + G(d,p) level of theory.

Structure	ΔH° (kJ mol^{-1}) 298 K	ΔS° (J mol^{-1} K^{-1}) 298 K	ΔG° (kJ mol^{-1}) 298 K
1a	0.00	13.13	0.00
1b	1.08	12.43	1.29
2a	3.02	12.42	3.23
2b	4.07	11.39	4.59
3a	25.34	15.38	24.67
3b	26.06	14.55	25.64
4a	56.86	21.63	54.32
4b	59.41	21.82	56.82
5a	58.81	4.12	61.49
5b	54.26	1.81	57.63
6a	70.22	1.74	73.61
6b	57.53	0.00	61.45
7a	86.30	10.09	87.21
7b	83.26	9.82	84.25

Please cite this article in press as: B.E. Ziegler, et al., Int. J. Mass Spectrom. (2012), doi:10.1016/j.ijms.2012.02.025

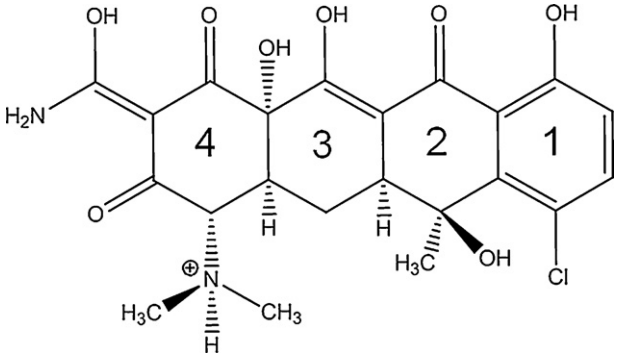

Fig. 2. Lowest energy form of protonated chlortetracycline.

described below. It is of considerable interest to note that, in all cases, the most energetically favourable form of the protonated species involves several subtle structural differences from the form shown in Fig. 1, as illustrated in the structure shown in Fig. 2. Firstly, the amide group is found to most favorably adopt an enol form of the amide with an orientation such that the enol OH hydrogen bonds to the carbonyl oxygen on the opposite side of ring 4 from the dimethyl amino functionality. Secondly, the enol of ring 4 becomes a carbonyl. The fact that the form shown in Fig. 1 represents the most stable structure of the neutral while that shown in Fig. 2 represents the most stable structure of the analogous protonated species, illustrates dramatically the subtle energetic interplay between keto and enol forms that can be provoked by protonation. This was confirmed computationally where the neutral form shown in Fig. 1 is found to be ~14 kJ mol^{-1} more energetically favourable than that of a neutral analogous to the ionic species shown in Fig. 2. Conversely, structures of ionic species analogous to the neutral in Fig. 1 were found to be higher in energy than the ionic structures described below.

In the work described here, protonated chlorotetracycline serves to illustrate the trends that are observed for the 6 tetracyclines investigated which will be presented in a future publication. It is important to note that even though the structures conventionally drawn to represent tetracyclines and their protonated forms appear to be planar, there is in fact considerable flexibility such that a near bowl-like shape is adopted, as illustrated in Fig. 3.

As noted above, the most favourable protonation site of each of the tetracycline derivatives is at the dimethyl amino

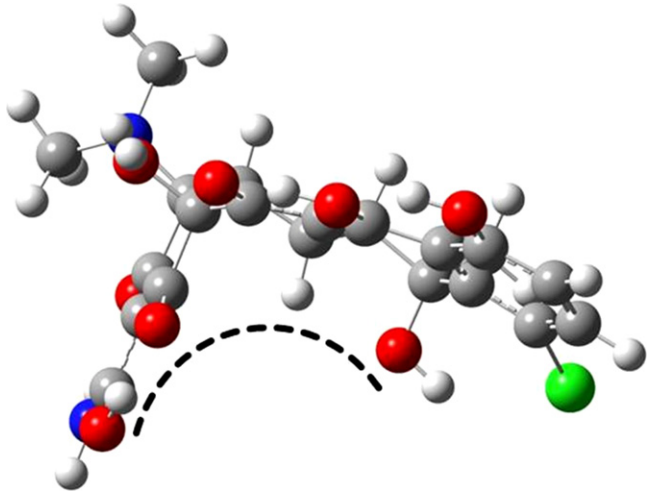

Fig. 3. Three dimensional structure of protonated chlortetracycline illustrating the bowl-like shape. The structure is optimized using the B3LYP/6-311 + G(d,p) level of theory.

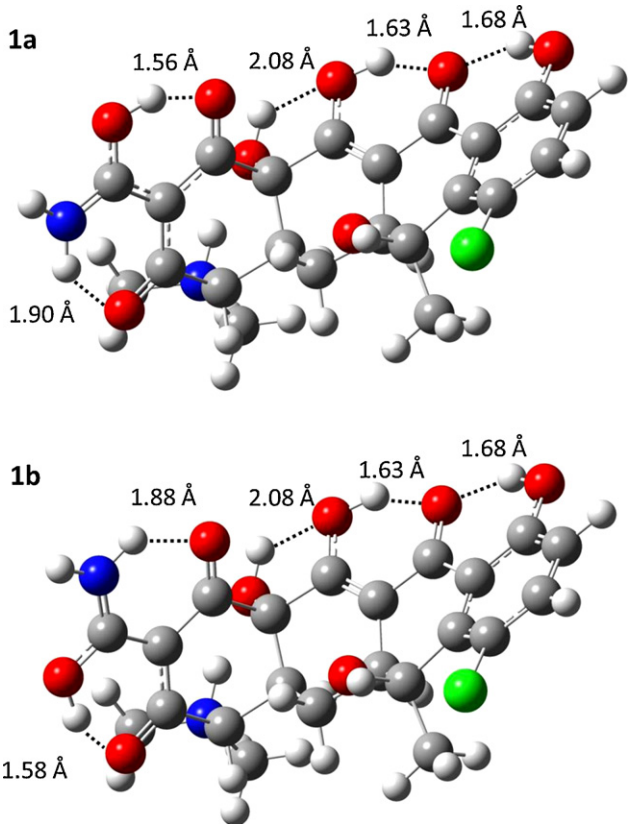

Fig. 4. Structure of protonated chlortetracycline forms **1a** and **1b**. The structures are optimized using the B3LYP/6-311 + G(d,p) level of theory.

nitrogen. However, there is, in addition, a very interesting pattern of intramolecular hydrogen bonds which can occur and which, if varied, can lead to subtle changes in the energetics. Firstly, as shown in Fig. 4, in the most favourable hydrogen bond orientation (**1a**), the hydroxyl hydrogen of the amide enol moiety is intramolecularly hydrogen bonded to the carbonyl oxygen of ring 4 opposite to the amino group (1.56 Å), while a single hydrogen of the NH_2 moiety of the amide enol is hydrogen bonded to the carbonyl oxygen of ring 4, adjacent to the dimethyl amino group (1.90 Å). As well, the hydroxyl groups of rings 1 and 3 orient themselves in such a way that the hydrogen of the hydroxyl on ring 1 forms an intramolecular hydrogen bond to the oxygen of the carbonyl group of ring 2 (1.68 Å) and in turn the hydrogen of the enol of ring 3 also forms an intramolecular hydrogen bond to the carbonyl oxygen of ring 2 (1.63 Å). At the same time, the hydroxyl group hydrogen at the junction of rings 3 and 4 also forms an intramolecular hydrogen bond to the enol oxygen of ring 3 (2.08 Å).

A second structure (**1b**), virtually identical in energy (ΔG° = 1.4 kJ mol^{-1} at 298 K), can be obtained by a 180° rotation of the amide enol group where the number and type of intramolecular hydrogen bonds remains the same (Fig. 4). The subtle reason for the energetic difference between **1a** and **1b** might best be understood from an examination of the key hydrogen bond distances. The lengths of the hydrogen bonds involving the oxygens in rings 1, 2 and 3 remain essentially unchanged while those involving the amide enol group do change. The amide enol hydrogen to carbonyl oxygen distance decreases by 0.2 Å and the enol hydrogen to carbonyl oxygen distance increases by 0.2 Å. Thus the very slight differences in the energetics are a result of the extremely subtle differences in the hydrogen bond environments.

The subtlety of hydrogen bond energetics coupled with the possibilities of several keto-enol tautomerisms on rings 1, 2 and 3

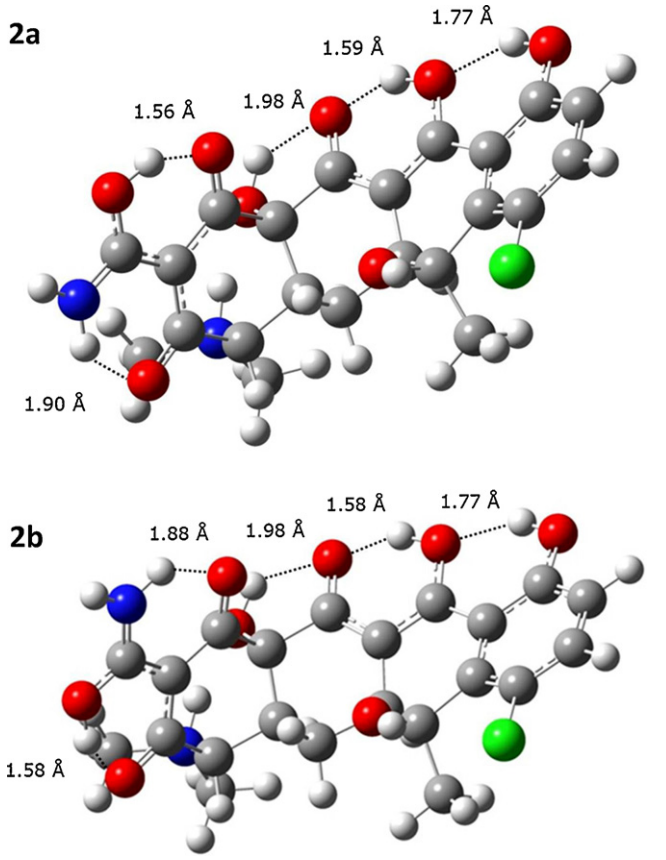

Fig. 5. Structure of protonated chlortetracycline forms **2a** and **2b**. The structures are optimized using the B3LYP/6-311 + G(d,p) level of theory.

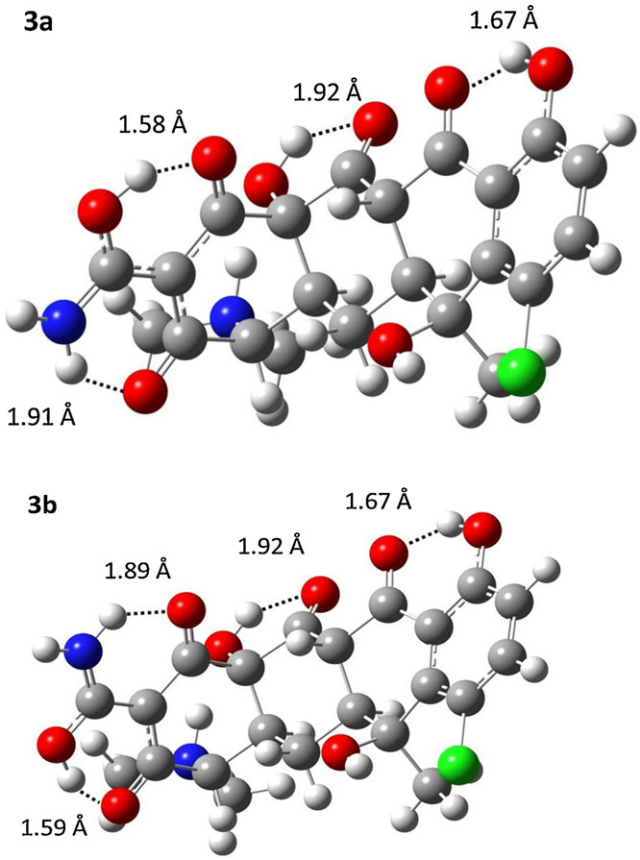

Fig. 6. Structure of protonated chlortetracycline forms **3a** and **3b**. The structures are optimized using the B3LYP/6-311 + G(d,p) level of theory.

therefore suggested a systematic computational analysis of such structural variants. For example, as shown in Fig. 5, structure **2a** differs from **1a** only in the keto-enol pattern of rings 2 and 3 and the hydrogen bonds involving the amide enol moiety remain unchanged. However, in **2a**, the exocyclic oxygen of ring 2 becomes an enol and that of ring 3 becomes a keto group. In so doing, the hydrogen bond between the oxygens of rings 1 and 2 increases by 0.09–1.77 Å, and that between the oxygens of rings 2 and 3 decreases by 0.04–1.59 Å. In addition the hydrogen bond from the hydroxyl of ring 4 to the exocyclic carbonyl oxygen of ring 3 decreases by 0.10–1.98 Å, however this hydrogen bond is much weaker and plays a more minor role in the relative stabilities. Thus even though there is a net decrease in the sum of hydrogen bond lengths in **2a** relative to **1a**, there is a very slight increase in free energy of 3.2 kJ mol^{-1}. This suggests that, despite the overall cumulative hydrogen bond distances, there is a slight energetic preference for enol to keto hydrogen bonds over enol to enol hydrogen bonds. The same pattern is repeated in a comparison of the amide enol rotated structures **2b** and **1b**.

The next most stable structure found also involves an additional enol to keto transformation. Relative to **2a**, the new structure **3a** (Fig. 6) is the result of an enol to keto transformation at ring 2. This decreases the number of hydrogen bond possibilities involving the exocyclic ring oxygens by one with a net increase in free energy of 24.7 kJ mol^{-1} relative to **1a**. However, the new enol to keto hydrogen bond distance between rings 1 and 2 in 3a is 0.1 Å shorter than the analogous enol to enol hydrogen bond distance seen in **2a** while nearly identical (within 0.01 Å) to the enol to keto hydrogen bond distance in **1a**. There is also a decrease in the hydrogen bond distance from the hydroxyl of ring 4 to the carbonyl of ring 3 of 0.06 Å relative to **2a**. Slight increases in the hydrogen bond distances involving the amide enol also result. Again these data reveal the preference for enol to keto hydrogen bonds.

The importance of the type of intramolecular hydrogen bonding involved is further demonstrated by the energetics and structure (Fig. 7) of the next most stable form of dimethylamino protonated chlortetracycline (**4a**) in which the keto and enol sites remain the same and the enol-amide orientation remains as in **2a**. However, the orientation of hydrogen bonds formed on rings 1, 2, and 3 are significantly different. No significant changes occur in the hydrogen bonds involving the amide enol nor that from the hydroxyl of ring 4 to the carbonyl of ring 3. The very significant change is the rotation

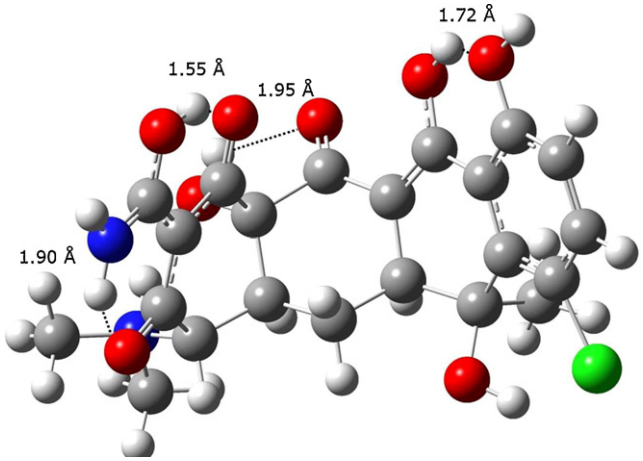

Fig. 7. Structure of protonated chlortetracycline form **4a**. The structure is optimized using the B3LYP/6-311 + G(d,p) level of theory.

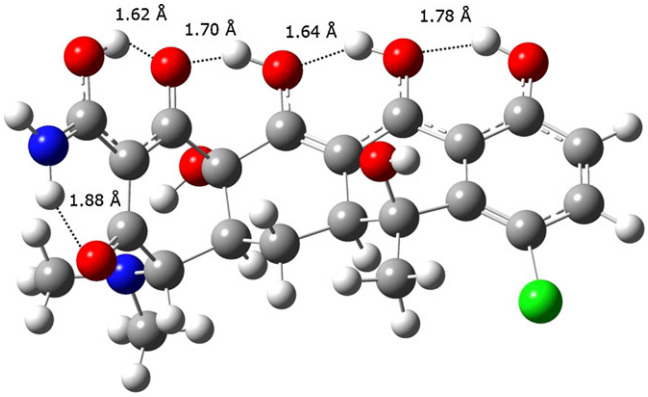

Fig. 8. Structure of protonated chlortetracycline form **5a**. The structure is optimized using the B3LYP/6-311+G(d,p) level of theory. Protonation occurs at the ring 3 carbonyl oxygen.

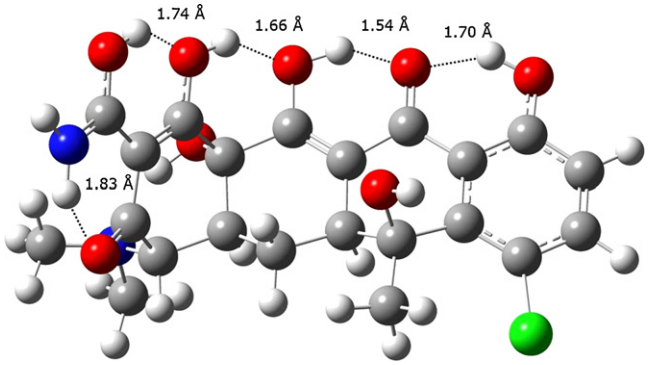

Fig. 9. Structure of protonated chlortetracycline form **6a**. The structure is optimized using the B3LYP/6-311+G(d,p) level of theory. Protonation occurs at the ring 4 carbonyl oxygen.

of the two enol groups such that a single enol to carbonyl hydrogen bond is lost. The new enol to enol hydrogen bond in **4a** is 0.05 Å shorter than that in **2a** while the free energy of **4a** is 51.1 kJ mol^{-1} greater than that of **2a**. This value might then be taken as a lower limit on the energy of the enol to carbonyl hydrogen bond in this structure. In **4b** the amide enol is rotated by 180° resulting in an approximate increase of 2.5 kJ mol^{-1} in energy relative to **4a**.

All other possible combinations of keto-enol tautomerism at rings 1, 2 and 3 were also investigated however none of these was within 100 kJ mol^{-1} of the lowest energy structure. This can be readily understood from the fact that a structure containing three enols is not possible since there is not an accessible hydrogen to accomplish this. All other permutations would involve a keto group at ring 1 which would necessarily lead to a loss of aromaticity of ring 1 which would be exceedingly energy costly.

Protonation at other sites of the molecule can also occur as illustrated by structure **5a** (Fig. 8) in which protonation occurs at the ring 3 carbonyl oxygen. In addition, in **5a**, each of the hydroxyl groups on rings 1, 2, and 3 are aligned in such a way as to give the maximum possible intramolecular hydrogen bonding, including an additional interaction between the added proton on the ring 3 carbonyl and the oxygen of the ring 4 carbonyl. Simultaneously, a hydrogen bond interaction exists between the amino group of the amide enol and the oxygen of ring 4 carbonyl. At ~60 kJ mol^{-1} higher in energy than **1a**, this structure is only marginally less stable than structure **4a**. A slight variation on structure **5a** is found in structure **5b** in which the amide enol group is rotated by 180° to give a hydrogen bond interaction between the enol hydroxyl hydrogen and the carbonyl oxygen of ring 4. In addition, the hydroxyl group at the junction of rings 3 and 4 can hydrogen bond to the dimethyl amino nitrogen with an O–H···N bond distance of 1.93 Å. As noted below, this O–H···N hydrogen bond motif is repeated in all structures in which protonation does not occur at the dimethyl amino nitrogen. The difference in stability of **5a** and **5b** is thus due to the subtle balance of hydrogen bond interactions between the amine and hydroxyl hydrogens of the amide enol with the two different adjacent ring 4 carbonyls. It is interesting to note that, in the absence of protonation on the dimethyl amino group, the most favourable orientation of the amide enol functionality is reversed as seen by the 2.9 kJ mol^{-1} difference in energy of **5b** relative to **5a**.

In structure **6a** (Fig. 9) protonation occurs at the "top" ring 4 carbonyl oxygen and results in a new hydrogen bond to the ring 3 carbonyl oxygen while maintaining the hydrogen bond between the oxygens of rings 2 and 3 and those of rings 1 and 2. Interestingly, protonation at the carbonyl of ring 4 leads to a structure in which, effectively, an intramolecular proton transfer has occurred from the enol of ring 2 to the carbonyl of ring 3 resulting in a configuration more closely resembling that shown of the neutral in Fig. 1. In this case the intramolecular hydrogen bond between the hydroxyl at the junction of rings 3 and 4 and the dimethyl amino nitrogen has a O–H···N distance of 1.90 Å. In structure **6b** the amide enol is again rotated by 180° resulting in the approximately 12 kJ mol^{-1} difference which is analogous, although somewhat larger, to that discussed above for **5b**.

A very different type of structure, **7a**, results from protonation at the carbon of the double bond at the junction of rings 2 and 3. This structure (Fig. 10) retains all of the intramolecular hydrogen bonds described above for **2a** with the exception of that involving the hydrogen of the hydroxyl group at the junction of rings 3 and 4. In **2a** the hydrogen of this hydroxyl group was hydrogen bonded to the carbonyl oxygen of ring 3 whereas in **5a** this hydrogen is now hydrogen bonded to the dimethyl amino nitrogen with an O–H···N bond distance of 1.78 Å. Again, in **7b**, rotation of the amide enol group results in the subtle variation of approximately 3 kJ mol^{-1} in stability.

Comparison of vibrational spectra generated *via* IRMPD with those obtained computationally aids in providing confirmation of structure. It is important to note at the outset however that the application of the Lorentzian line widths to the computed frequencies and intensities results in shifts in the maxima observed in the computed spectrum from those of the calculated line spectra, especially where there are peaks of high intensity relatively close in frequency.

The two lowest free energy structures, **1a** and **1b** would reasonably be expected to give the best-match when compared to the IRMPD spectrum and this comparison is shown in Fig. 11. The spectra of **1a** and **1b** can be seen to be very similar, as would be

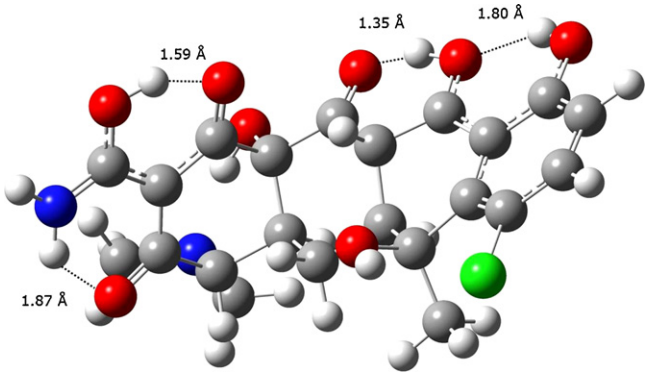

Fig. 10. Structure of protonated chlortetracycline form **7a**. The structure is optimized using the B3LYP/6-311+G(d,p) level of theory. Protonation occurs at the carbon at the ring 2,3 junction nearest the exocyclic oxygens.

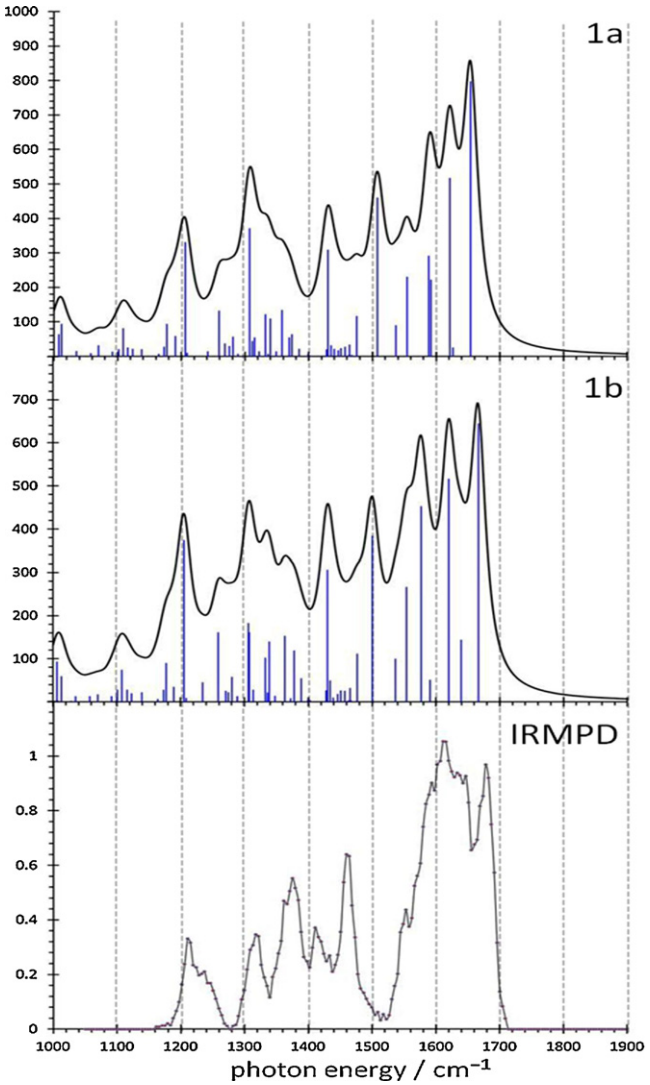

Fig. 11. Comparison of the IRMPD spectrum of protonated chlortetracycline with calculated harmonic spectra (B3LYP/6-311 + G(d,p)) of the two lowest energy isomers, **1a** and **1b**. Absolute intensities for the calculated spectra are represented by vertical blue lines (km mol^{-1}) and the intensity of the IRMPD spectrum is expressed as the fragmentation efficiency (P_{frag}).

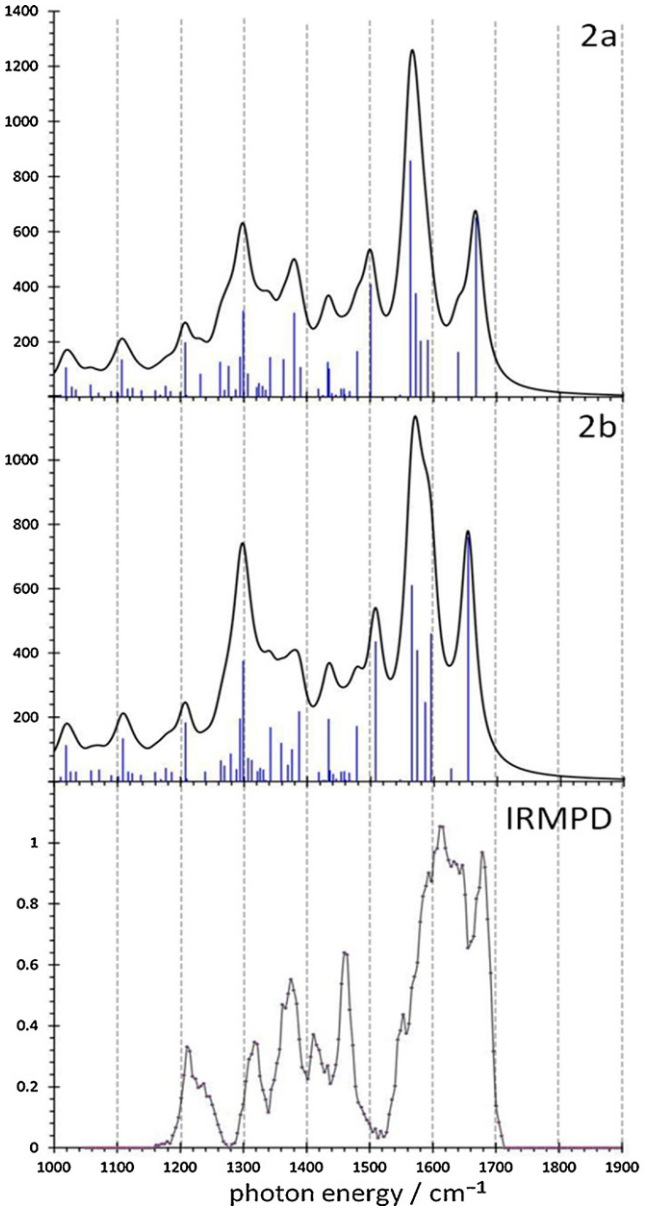

Fig. 12. Comparison of the IRMPD spectrum of protonated chlortetracycline with calculated harmonic spectra (B3LYP/6-311 + G(d,p)) of the two isomers, **2a** and **2b**. Absolute intensities for the calculated spectra are represented by vertical blue lines (km mol^{-1}) and the intensity of the IRMPD spectrum is expressed as the fragmentation efficiency (P_{frag}).

expected based on the fact that the only real difference between the two isomers involves the orientation of the amide enol moiety with, however, the same number and type of hydrogen bonds. The number and proximity of vibrational modes in the computed spectra would suggest that, given the experimental resolution of ~20 cm^{-1}, there is little chance that peaks will be well resolved as is seen to be the case in the experimental IRMPD spectrum [34]. Even so, it can be seen that the features predicted by the computed spectrum are present, and match well in both frequency and relative intensities those of the computed spectrum. The broad feature from 1550 to 1700 cm^{-1} can be considered to be the most diagnostic in terms of differentiating among the possible structures. In terms of assigning modes to this feature, the experimental spectrum corresponds most likely to a composite of 5 peaks at 1553, 1588, 1592, 1621 and 1654 cm^{-1} obtained from the computed spectrum of **1a**. Each of these peaks involves complex combination of modes involving parts of the structure. The peak at 1654 cm^{-1} is computed to have the largest intensity of any of the modes in the 1000–2000 cm^{-1} region of the spectrum and this is consistent with the relatively sharp feature observed at ~1680 cm^{-1} in the experimental IRMPD spectrum. This peak is largely associated with concerted motion of all of the atoms of the amide enol group, including those to which hydrogen bonding occurs. The strong peak at 1621 cm^{-1} is primarily due to a concerted stretching motion of all of the atoms connecting the keto moiety of ring 2 and the enol moiety of ring 3. The calculated peaks at 1588 and 1592 cm^{-1} both involve multiple complex stretching and bending motions, primarily but not exclusively, of the extensive hydrogen bonded network of the molecule, spanning from ring 1 through ring 4. The peak at 1553 cm^{-1} is largely associated with large amplitude motions around the hydrogen bonds of the hydroxyl groups of rings 1 and 3, as well as stretching motions of the aromatic ring. Analogous assignments can be made for the peaks at 1553, 1576, 1620, 1639 and 1666 cm^{-1}, respectively found for structure **1b**.

Structures **2a** and **2b**, which are only 3 kJ mol^{-1} higher in energy that **1a** and **1b**, might also be expected to be present in the experimental spectrum of the electrosprayed protonated

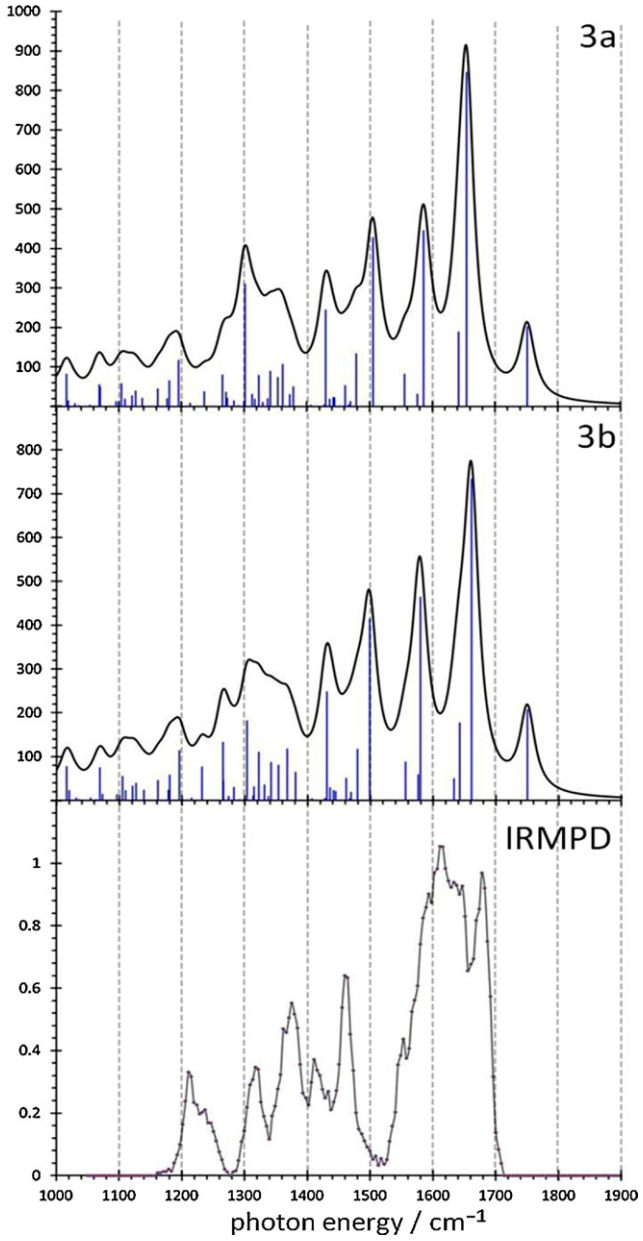

Fig. 13. Comparison of the calculated harmonic spectra (B3LYP/6-311 + G(d,p)) of isomers **3a**, and **3b** in the 1000–2000 cm^{-1} region. Absolute intensities are represented by vertical blue lines (km mol^{-1}).

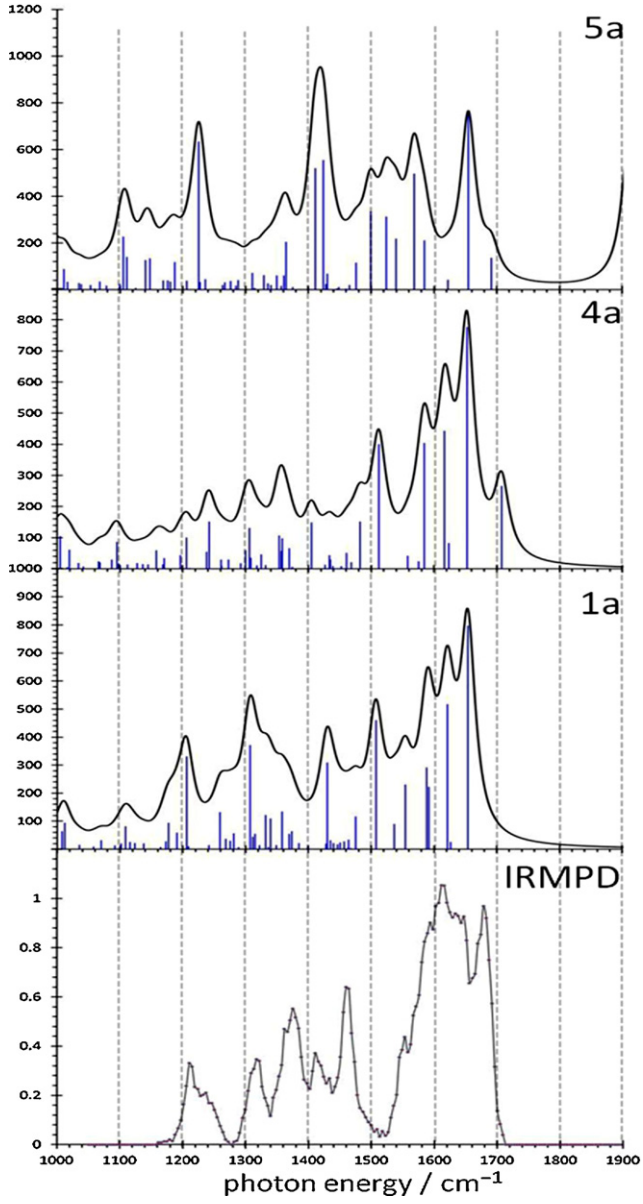

Fig. 14. Comparison of the calculated harmonic spectra (B3LYP/6-311 + G(d,p)) of isomers **1a**, **4a** and **5a** in the 1000–2000 cm^{-1} region. Absolute intensities are represented by vertical blue lines (km mol^{-1}).

chlorotetracycline on purely energetic grounds. As can be seen from a comparison of Figs. 11 and 12, there are peaks of relatively high intensity in the same general frequency ranges for these species and the experimental spectrum might well best be regarded as a composite of the two general structural motifs. Similar assignments of the modes as those described above for **1a** also apply to **2a** and **2b** for the 1550–1700 cm^{-1} region. However, since **1a** and **1b** most closely resemble the structure assigned to protonated chlorotetracyline in the solid phase and solution, it is possible that this structure is maintained in the transfer to the gas phase *via* electrospray ionization. PCM calculations were carried which support that this form of the protonated species is indeed the most stable in solution.

In contrast, the experimental and computed spectra for the next highest energy structures are seen to exhibit greater differences between vibrational signatures than those found for the lowest energy structure, indicating that these structures are likely not present in any appreciable abundance in the experimental IRMPD spectrum. For example, as seen in Fig. 13, the dominant feature for structure **3a** calculated above 1600 cm^{-1} is less complex and is shifted generally to higher frequency compared to the experimental spectrum and compared to that found in structures **1a** and **1b**. In addition a peak is predicted at 1750 cm^{-1} which is not seen in the experimental IRMPD spectrum. In addition, at 25 kJ mol^{-1} higher in energy that **1a**, it is unlikely that this species would be present.

Similarly the spectra of structures **4a**, **4b**, **5a**, and **5b** (Fig. 14) also exhibit higher frequency peaks relative to those of structures **1a** and **1b**. For example, as seen in Fig. 14, the calculated spectrum for structure **5a** shows a strong peak at 1975 cm^{-1} that is absent in the experimental spectrum. All of the structures 4 through 7, involve protonation at sites other than the dimethyamino group and are thus extremely unlikely to have been generated in the electrospray process.

Thus, the IRMPD spectrum and calculated spectra strongly support the existence of protonated chlortetracycline as a combination

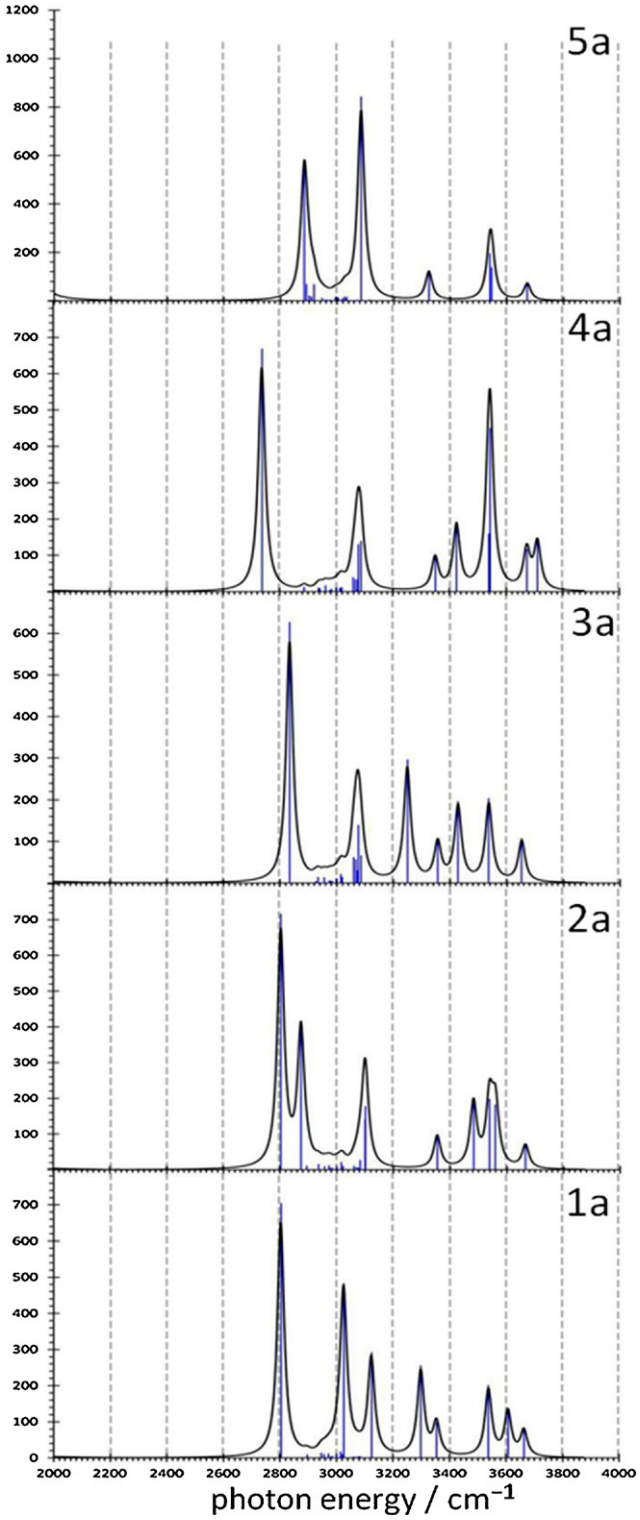

Fig. 15. Comparison of the calculated harmonic spectra (B3LYP/6-311 + G(d,p)) of isomers **1a** through **5a**, inclusive, in the 2000–4000 cm^{-1} region. Absolute intensities are represented by vertical blue lines (km mol^{-1}).

of the two lowest energy computed structures, **1a** and **1b** with the possibility that **2a** and **2b** might also be present.

To be even more confident that the most energetically favourable gas phase structures of these protonated tetracycline derivatives have been determined, it would be desirable to perform an analogous IRMPD experiment using an optical parametric oscillator (OPO) which is capable of scanning the range of 2000–4000 cm^{-1}. Such an experiment would give further confirmation of the structure observed since, as can be seen in Fig. 15, the computed spectra of **1a**, **2a**, **3a**, **4a** and **5a** are markedly different in this region.

4. Conclusion

The IRMPD spectrum of protonated chlortetracycline has been obtained. Energetics and vibrational frequencies were calculated at the B3LYP/6-311 + G(d,p) level of theory for several possible isomeric and tautomeric forms and the spectra have been compared to the IRMPD spectrum. The results suggest that the most energetically favourable protonation site is at the dimethyl amine moiety for each of the most stable species, which are tautomeric variants. It is also interesting to note that the most energetically favourable structures adopt a bowl-like shape as a result of the hydrogen bonded enol form of the amide. As well, in the most stable structures, two hydroxyl groups of rings 1, 2 and 3 are oriented in such a way as to maximize the hydrogen bonding possibilities.

Acknowledgements

Generous financial support of this work by the Natural Sciences and Engineering Research Council of Canada (NSERC) is gratefully acknowledged. We are also very grateful for the valuable assistance of the CLIO team and the CLIO technical support staff, for their outstanding assistance and kind hospitality during our stay in Orsay.

This manuscript is dedicated to Professor Alex Harrison on the occasion of his 80th birthday. TBM is especially grateful for the inspiration provided during the early stages of his career by Alex's many insightful contributions to gas phase ion chemistry.

References

[1] B.M. Duggar, Annals of the New York Academy of Sciences 51 (1948).
[2] J.H. Boothe, J. Morton, J.P. Petisi, R.G. Wilkinson, J.H. Williams, Journal of the American Chemical Society 75 (1953).
[3] L.H. Conover, W.T. Moreland, A.R. English, C.R. Stephens, F.J. Pilgrim, Journal of the American Chemical Society 75 (1953).
[4] R. Blackwood, J.J. Beereboom, C.R. Stephens, H.H. Rennhard, M.S. Wittenau, Journal of the American Chemical Society 83 (1961).
[5] M.J. Martell, J.H. Boothe, Journal of Medicinal Chemistry 10 (1967).
[6] C.R. Stephens, P.N. Gordon, R.K. Blackwood, M.S. Wittenau, K. Murai, H.H. Rennhard, J.J. Beereboom, Journal of the American Chemical Society 85 (1963).
[7] I. Chopra, M. Roberts, Microbiology and Molecular Biology Reviews 65 (2001).
[8] I. Chopra, P.M. Hawkey, M. Hinton, Journal of Antimicrobial Chemotherapy 29 (1992).
[9] I. Chopra, Antimicrobial Agents and Chemotherapy 38 (1994).
[10] D. Schnappinger, W. Hillen, Archives of Microbiology 165 (1996).
[11] J. Bordner, Acta Crystallographica Section B-Structural Science 35 (1979).
[12] W. Clegg, S.J. Teat, Acta Crystallographica Section C-Crystal Structure Communications 56 (2000).
[13] M.J. Frisch, G.W. Trucks, H.B. Schlegel, G.E. Scuseria, M.A. Robb, J.R. Cheeseman, G. Scalmani, V. Barone, B. Mennucci, G.A. Petersson, H. Nakatsuji, M. Caricato, X. Li, H.P. Hratchian, A.F. Izmaylov, J. Bloino, G. Zheng, J.L. Sonnenberg, M. Hada, M. Ehara, K. Toyota, R. Fukuda, J. Hasegawa, M. Ishida, T. Nakajima, Y. Honda, O. Kitao, H. Nakai, T. Vreven, J.A. Montgomery Jr., J.E. Peralata, F. Ogliaro, M. Bearpark, J.J. Heyd, E. Brothers, K.N. Kudin, V.N. Staroverov, R. Kobayashi, J. Normand, K. Raghavachari, A. Rendell, J.C. Burant, S.S. Iyengar, J. Tomasi, M. Cossi, N. Rega, J.M. Millam, M. Klene, J.E. Knox, J.B. Cross, V. Bakken, C. Adamo, J. Jaramillo, R. Gomperts, R.E. Stratmann, O. Yazyev, A.J. Austin, R. Cammi, C. Pomelli, J.W. Ochterski, R.L. Martin, K. Morokuma, V.G. Zakrzewski, G.A. Voth, P. Salvador, J.J. Dannenberg, S. Dapprich, A.D. Daniels, O. Farkas, J.B. Foresman, J.V. Ortiz, J. Cioslowski, D.J. Fox, Gaussian 09, Revision A.02, Gaussian Inc., Wallingford, CT, 2009.
[14] A.D. Becke, Journal of Chemical Physics 98 (1993).
[15] R.A. Marta, R.H. Wu, K.R. Eldridge, J.K. Martens, T.B. McMahon, International Journal of Mass Spectrometry 297 (2010).
[16] R.A. Marta, R.H. Wu, K.R. Eldridge, J.K. Martens, T.B. McMahon, Physical Chemistry Chemical Physics 12 (2010).
[17] S.M. Martens, R.A. Marta, J.K. Martens, T.B. McMahon, Journal of Physical Chemistry A 115 (2011).
[18] A.P. Scott, L. Radom, Journal of Physical Chemistry 100 (1996).

[19] J.E. Delbene, W.B. Person, K. Szczepaniak, Journal of Physical Chemistry 99 (1995).
[20] J.P. Merrick, D. Moran, L. Radom, Journal of Physical Chemistry A 111 (2007).
[21] R.H. Wu, T.B. McMahon, Journal of the American Chemical Society 129 (2007).
[22] R.H. Wu, T.B. McMahon, Chemphyschem 9 (2008).
[23] K. Rajabi, K. Theel, E.A.L. Gillis, G. Beran, T.D. Fridgen, Journal of Physical Chemistry A 113 (2009).
[24] T.R. Rizzo, J.A. Stearns, O.V. Boyarkin, International Reviews in Physical Chemistry 28 (2009).
[25] J.A. Stearns, C. Seaiby, O.V. Boyarkin, T.R. Rizzo, Physical Chemistry Chemical Physics 11 (2009).
[26] R.H. Wu, T.B. McMahon, Journal of Physical Chemistry B 113 (2009).
[27] M.K. Drayss, P.B. Armentrout, J. Oomens, M. Schaefer, International Journal of Mass Spectrometry 297 (2010).
[28] E.A.L. Gillis, T.D. Fridgen, International Journal of Mass Spectrometry 297 (2010).
[29] W.K. Mino, J. Szczepanski, W.L. Pearson, D.H. Powell, R.C. Dunbar, J.R. Eyler, N.C. Polfer, International Journal of Mass Spectrometry 297 (2010).
[30] J.S. Prell, T.G. Flick, J. Oomens, G. Berden, E.R. Williams, Journal of Physical Chemistry A 114 (2010).
[31] K. Rajabi, E.A.L. Gillis, T.D. Fridgen, Journal of Physical Chemistry A 114 (2010).
[32] D. Semrouni, O.P. Balaj, F. Calvo, C.F. Correia, C. Clavaguera, G. Ohanessian, Journal of the American Society for Mass Spectrometry 21 (2010).
[33] R.C. Dunbar, J.D. Steill, J. Oomens, Journal of the American Chemical Society 133 (2011).
[34] J.M. Ortega, F. Glotin, R. Prazeres, Infrared Physics & Technology 49 (2006).
[35] V.N. Dobrynin, A.I. Gurevich, M.G. Karapetyan, M.N. Kolosov, M.M. Shemyakin, Tetrahedron Letters (1962).
[36] J. Donohue, K.N. Trueblood, M.S. Webster, J.D. Dunitz, Journal of the American Chemical Society 85 (1963).
[37] A.F. Casy, A. Yasin, Journal of Pharmaceutical & Biomedical Analysis 1 (1983) 281.
[38] R.D. Curtis, R.E. Wasylishen, Canadian Journal of Chemistry-Revue Canadienne De Chimie 69 (1991).
[39] S. Mooibroek, R.E. Wasylishen, Canadian Journal of Chemistry-Revue Canadienne De Chimie 65 (1987).

Please cite this article in press as: B.E. Ziegler, et al., Int. J. Mass Spectrom. (2012), doi:10.1016/j.ijms.2012.02.025